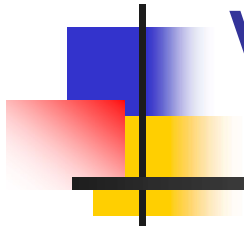# Contornos de grão
Vacâncias
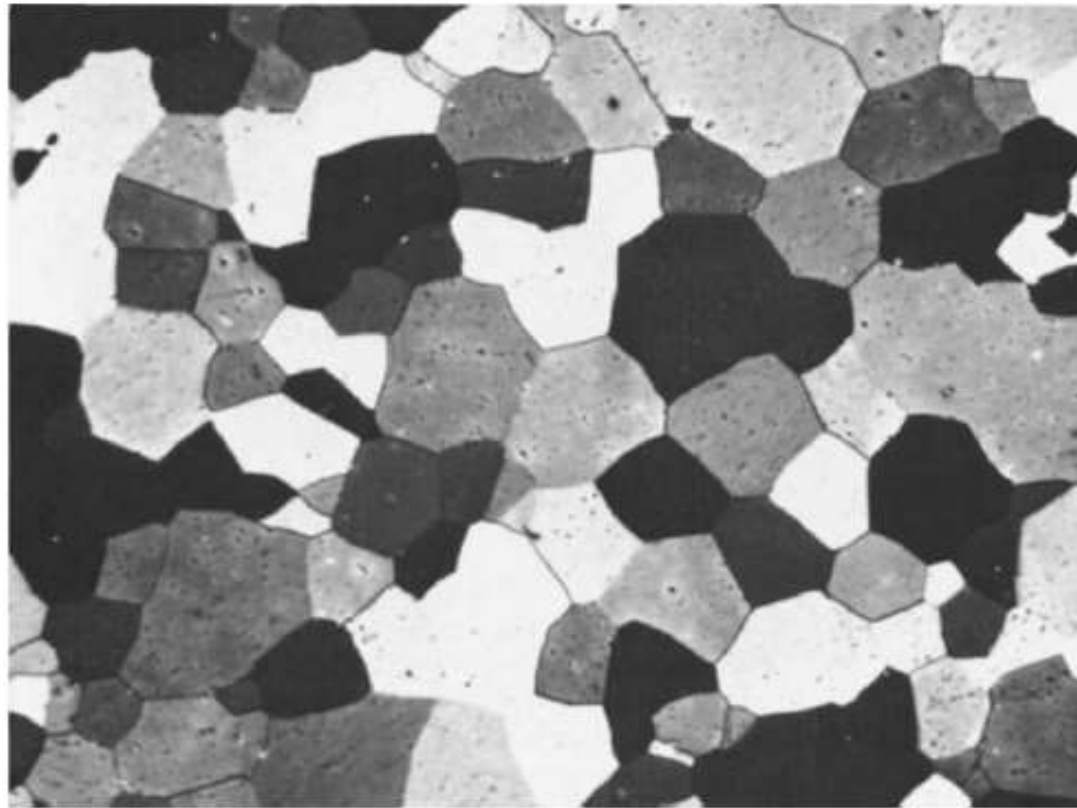
Metal policristalino

FIG. 6.1 A polycrystalline zirconium specimen photographed with polarized light. In this photograph, individual crystals can be distinguished by a difference in shading, as well as by the thin dark lines representing grain boundaries. 350×. Note that most of the triple junctions form 120° angles. (Photomicrograph by E. R. Buchanan.)

Contorno de baixo ângulo

$$\sin \theta/2 = b/2d \qquad\qquad 6.1$$

p/ θ pequeno:
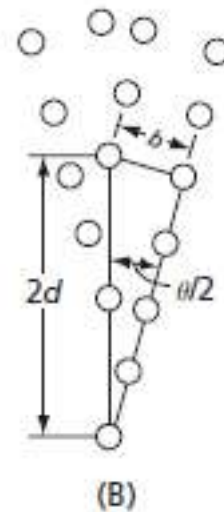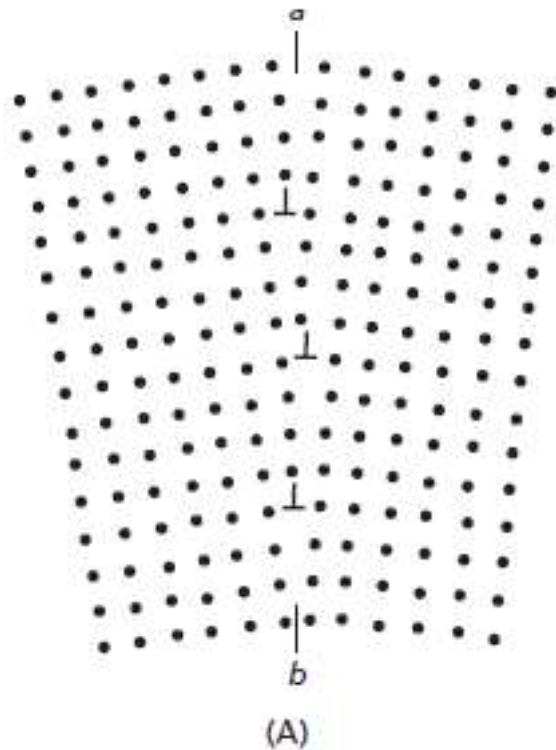
$$\theta = b/d$$

FIG. 6.2 (A) Dislocation model of a small-angle grain boundary. (B) The geometrical relationship between θ, the angle of tilt, and d, the spacing between the dislocations
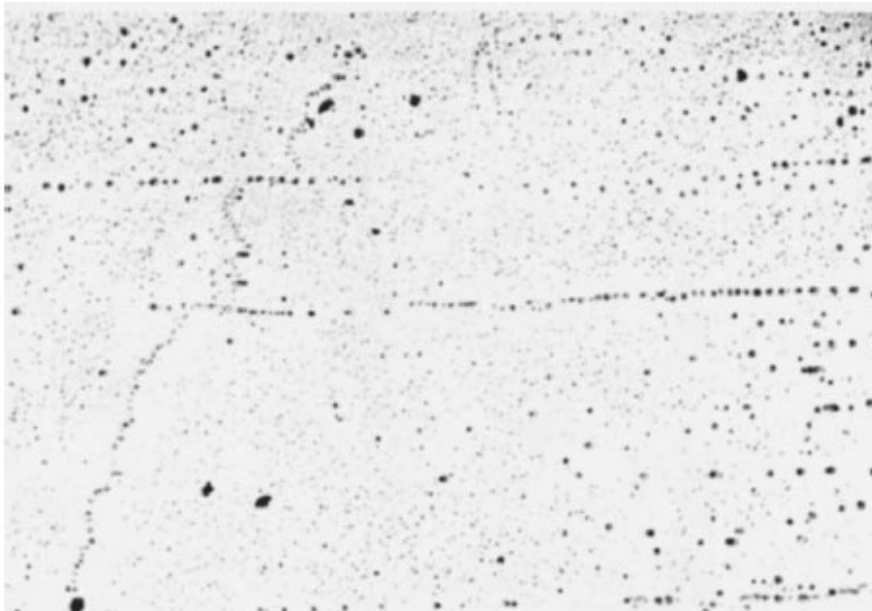
Contorno de baixo ângulo

FIG. 6.3 Low-angle boundaries in a magnesium specimen. The rows of etch pits correspond to positions where dislocations intersect the surface
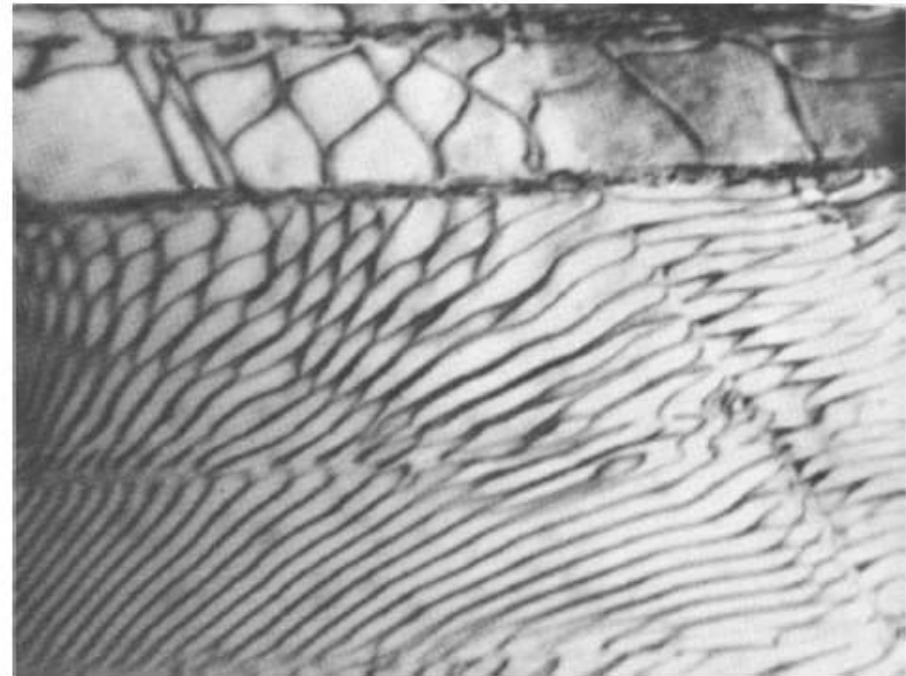

FIG. 6.4 A low-angle boundary in a copper—13.2 atomic percent aluminum specimen deformed 0.7 percent in tension as observed in the transmission electron microscope. This boundary has both a tilt and a twist character. Magnification: 32,000×. (Photograph courtesy of J. Kastenbach and E. J. Jenkins.)
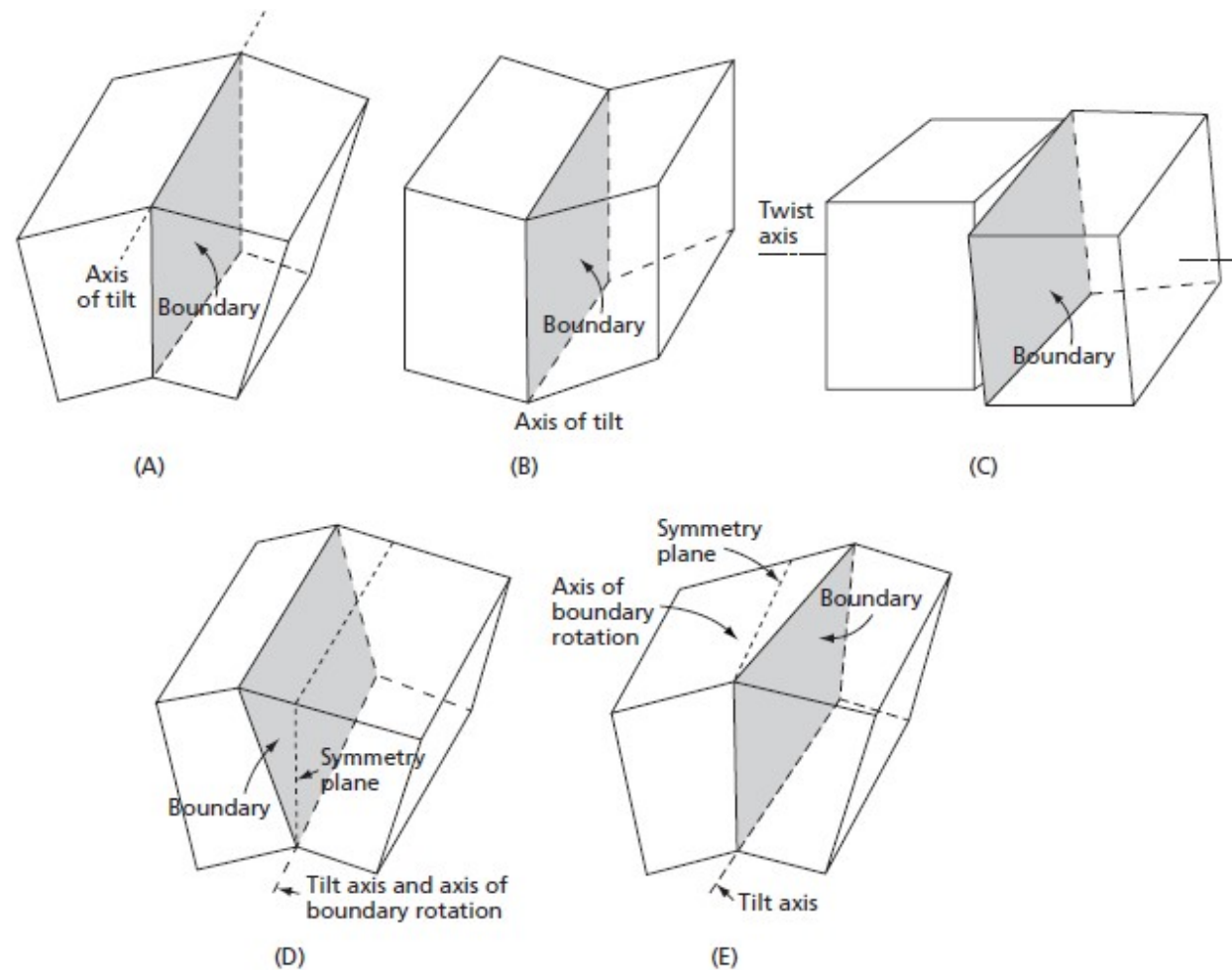
Graus de liberdade

FIG. 6.5 The five degrees of freedom of a grain boundary
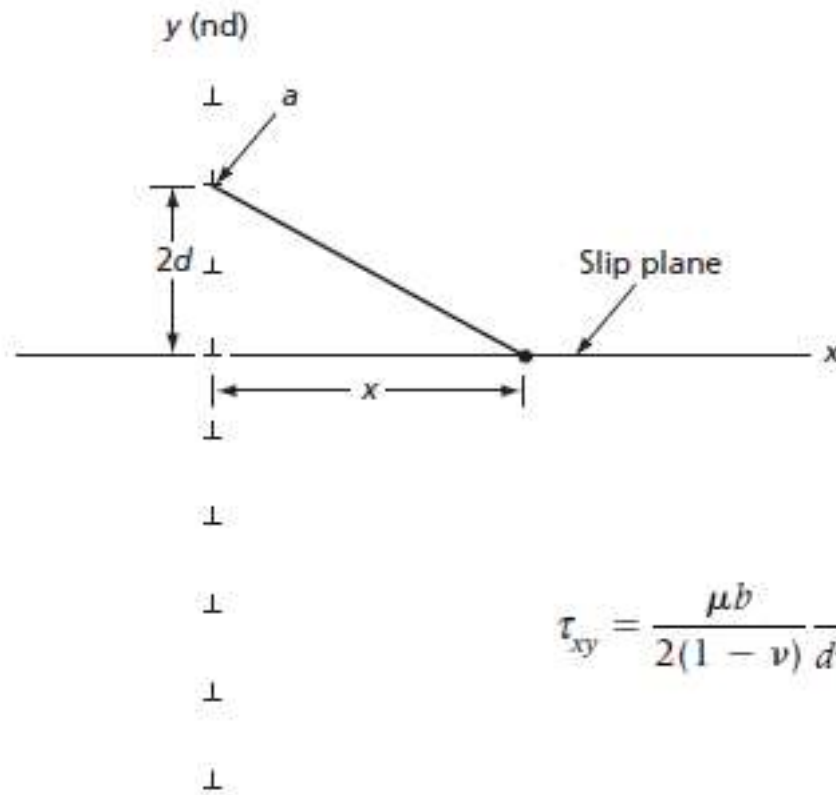
Campo de tensões

FIG. 6.6 A diagram defining the parameters used in computing the stress due to a simple tilt boundary. The y scale is in units of d, the distance between adjacent boundary dislocations, and n in the number

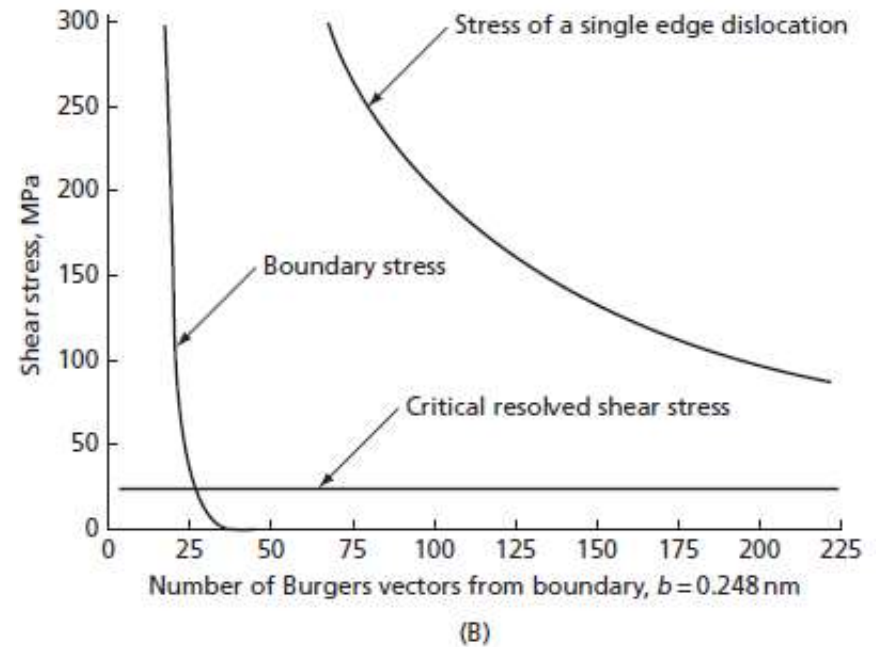$$\tau_{xy} = \frac{\mu b}{2(1-v)} \frac{\pi x}{d^2(\sinh^2(\pi x/d))}$$

Campo de tensões
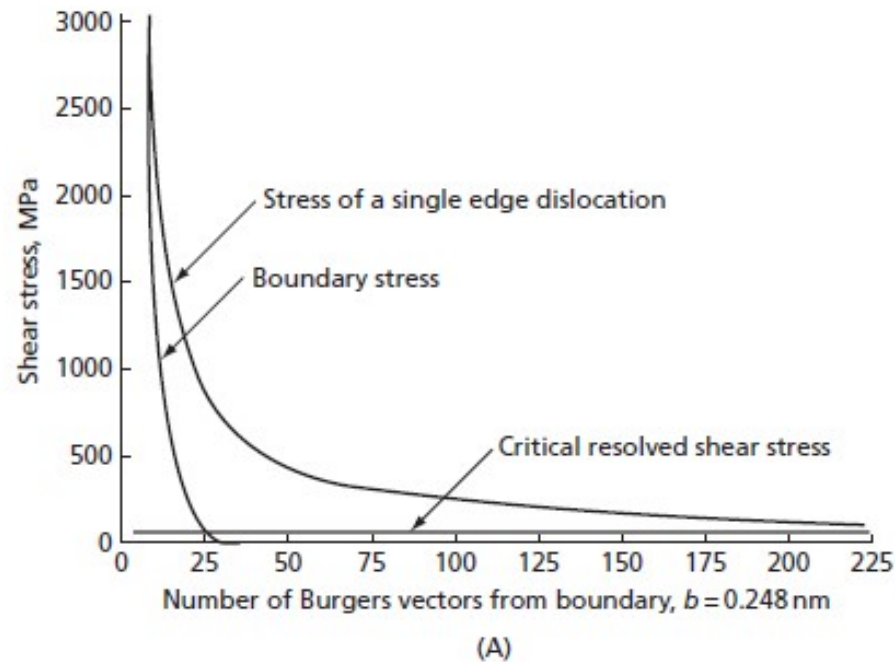

FIG. 6.7 (A) The stress, τ_{xy}, due to a tilt boundary and due to a single edge dislocation as functions of the distance measured in Burgers vectors. **(B)** Same as in (A) but at an expanded stress $d = 22b$

Energia

$$\gamma_b = w_{bd}/d = \frac{\mu b^2}{4\pi(1-v)} [\eta_0 \coth \eta_0 - \ln(2\sinh \eta_0)]$$

$$\gamma_b = \frac{\mu b}{4\pi(1-v)}\theta(\ln \alpha/2\pi - \ln \theta + 1)$$ p/ baixo ângulo
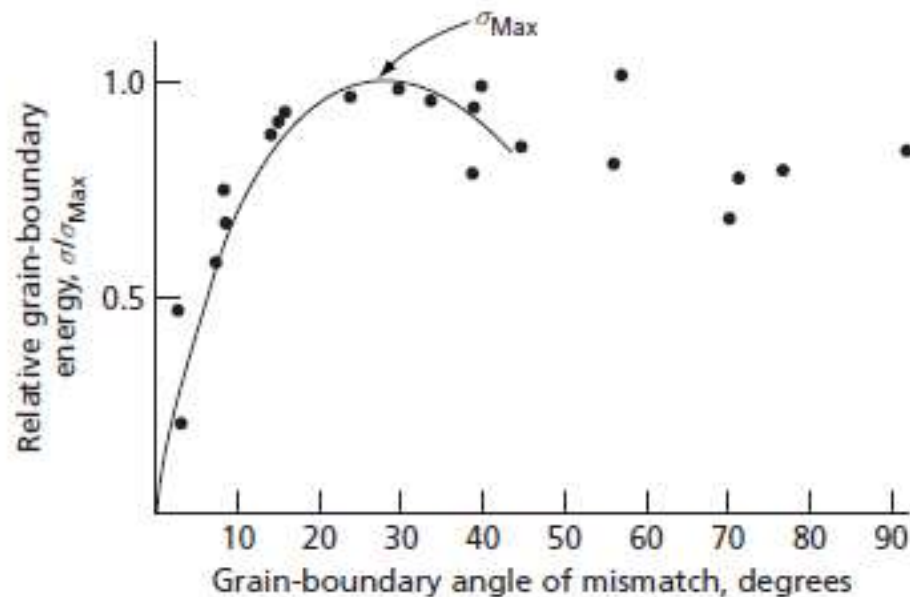

FIG. 6.8 Relative grain-boundary energy as a function of the angle of mismatch between the crystals bordering the boundary. Solid-line theoretical curve; dots experimental data of Dunn for silicon iron. (After *Dislocations* in *Crystals*, by Read, W. T., Jr. Copyright 1953. McGraw-Hill Book Co., Inc., New York.)
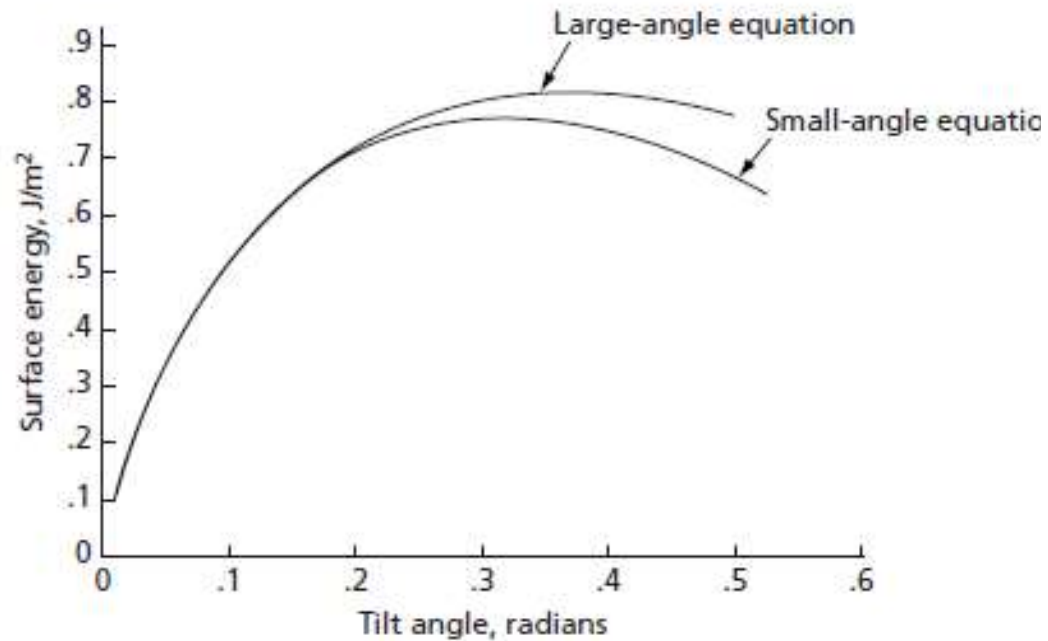
Energia

FIG. 6.10 The effect of α on the γ_b against θ curves

FIG. 6.9 The surface energy of a tilt boundary, γ_b, as a function of its angle of tilt, θ, as obtained with the small-angle and large-angle equations
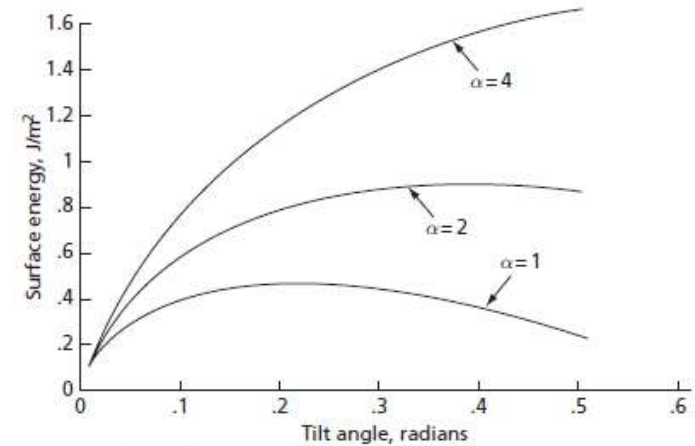
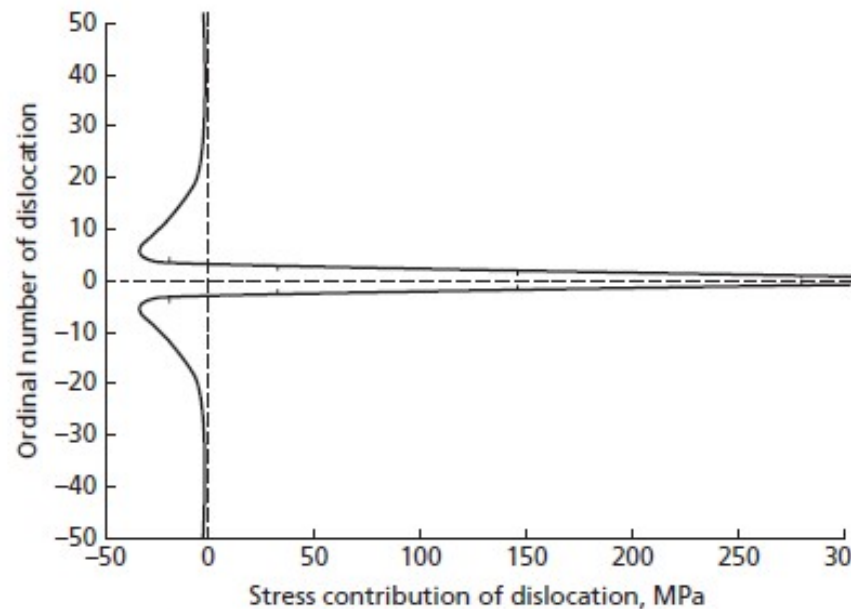# Estruturas de discordâncias com baixa energia (LEDS)

FIG. 6.11 The magnitude of the shear-stress contribution, at point x on the slip plane, of a dislocation in the tilt boundary as a function of its location in the boundary
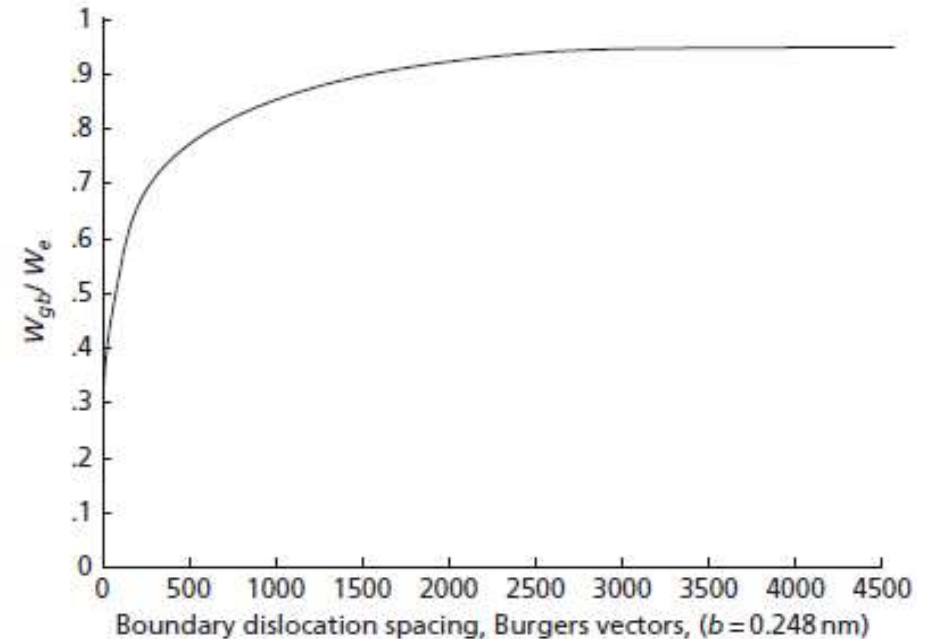
FIG. 6.12 The variation of W_{gb}/W_ℓ with the spacing between the dislocations in a tilt boundary

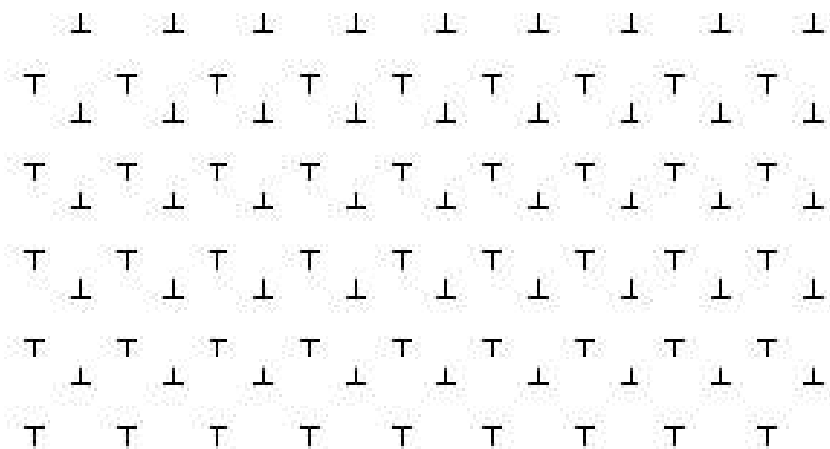# Estruturas de discordâncias com baixa energia (LEDS)
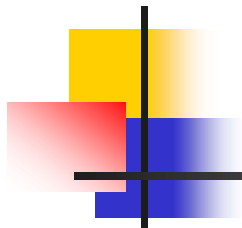
FIG. 6.13 The LEDS known as the Taylor lattice
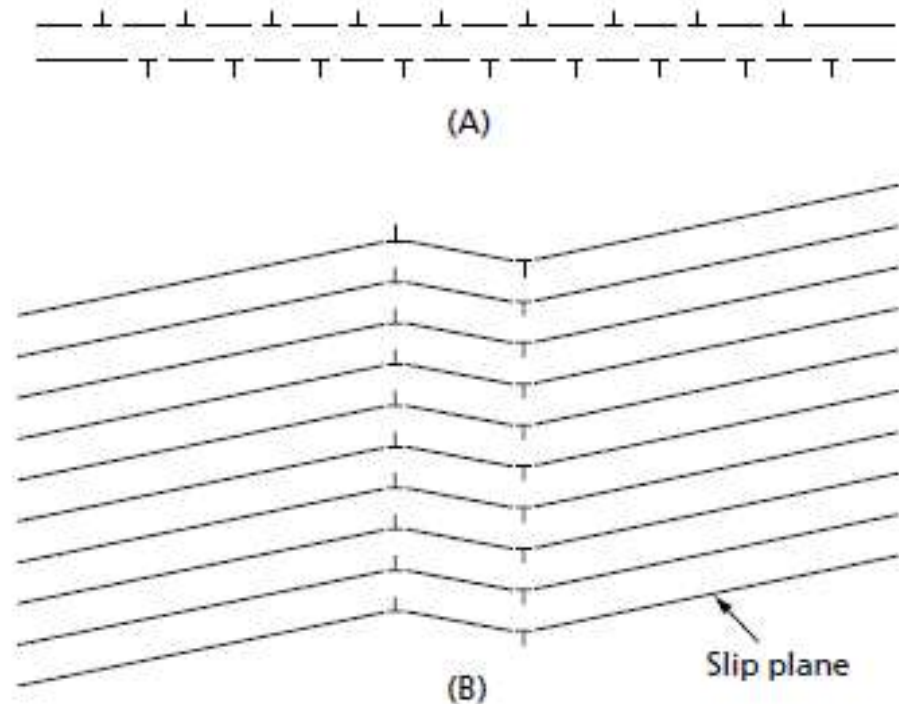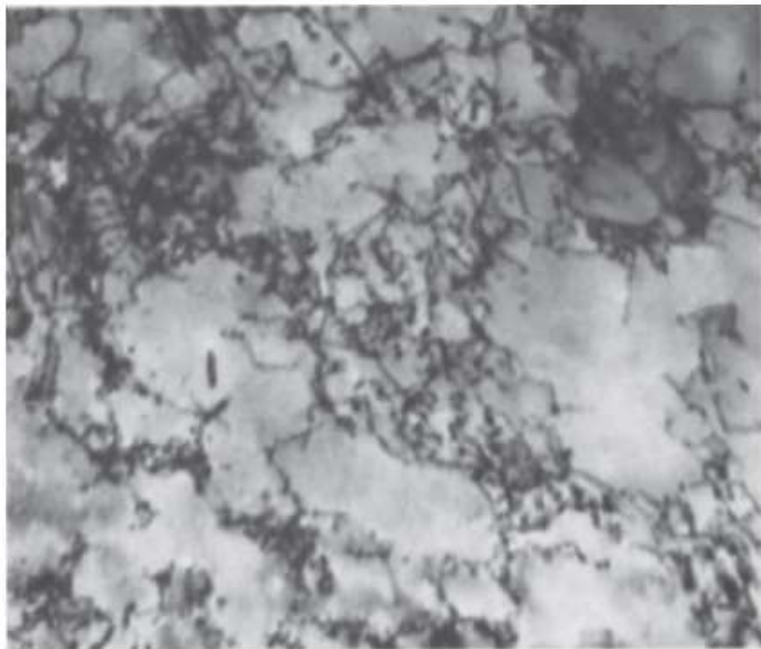

(A)

(B)

Slip plane

FIG. 6.14 (A) A dipolar mat that can form as a result of the interaction between dislocations of opposite sign moving on a pair of adjacent and parallel slip planes. (B) When a kink band forms in a crystal, a dipolar array of edge dislocations of a different type is created

Células (recuperação dinâmica)

(A) 9 percent strain

$$\vartheta = \kappa/\sqrt{\overline{\rho}}$$

Maior energia de falha de empilhamento maior tendência à recuperação dinâmica.
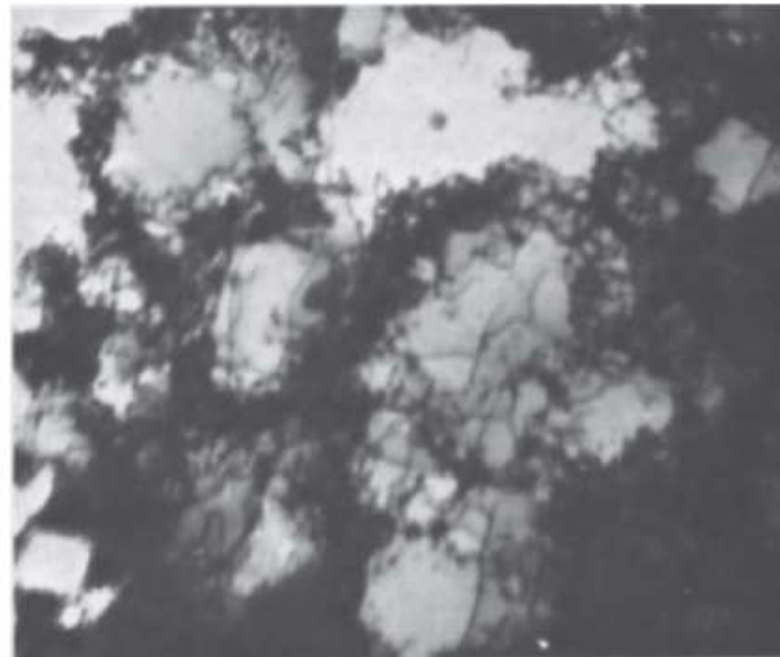
(B) 26 percent strain

FIG. 6.15 These transmission electron micrographs illustrate dynamic recovery in nickel deformed at 77 K. Note that even at this low temperature there is a definite tendency to form a cell structure that increases at high strains. (This material was published in Scripta Metallurgica, Vol. 4, Issue 10, W.P Longo and R.E. Reed-Hill, Work softening in polycrystalline metals, 765–770. Copyright Elsevier Science Ltd. (1970). http://www.sciencedirect.com/science/journal/00369748)

Células (recuperação dinâmica)

Efeito de
elementos de liga

FIG. 6.16 Alloying normally reduces the stacking-fault energy of a metal. This can have a pronounced effect on the dislocation structure, as can be seen in these two electron micrographs. **(A)** Pure nickel strained 3.1 percent at 293 K. Magnification: 25,000X. **(B)** Nickel – 5.5 wt. percent aluminum alloy strained 2.7 percent at 293 K. Magnification: 37,500X. (Photographs courtesy of J. O. Stiegler, Oak Ridge National Laboratories, Oak Ridge, Tenn.)
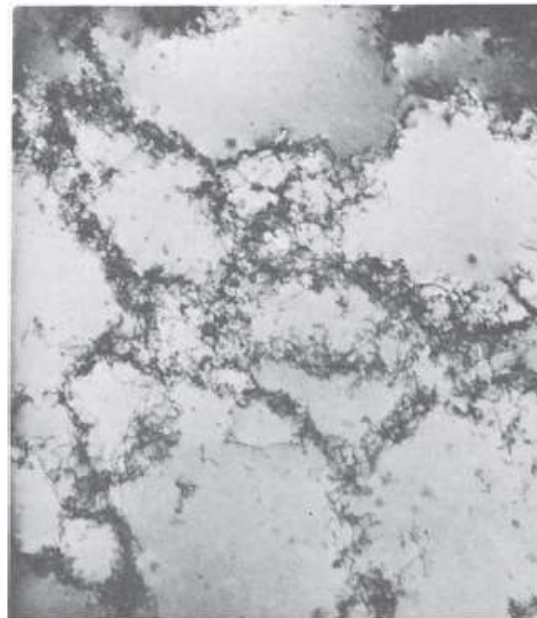
(A)

(B)

Tensão superficial

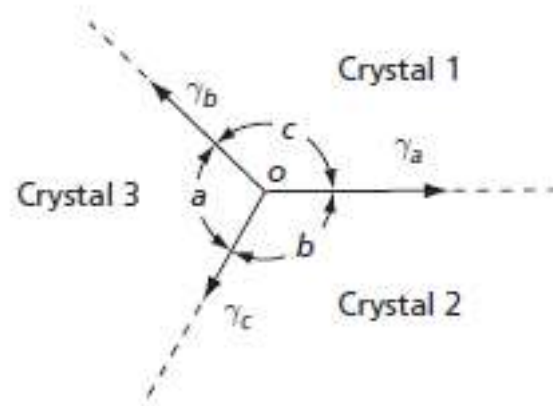$$\frac{\gamma_a}{\sin a} = \frac{\gamma_b}{\sin b} = \frac{\gamma_c}{\sin c}$$

FIG. 6.17 The grain-boundary surface tensions at a junction of three crystals
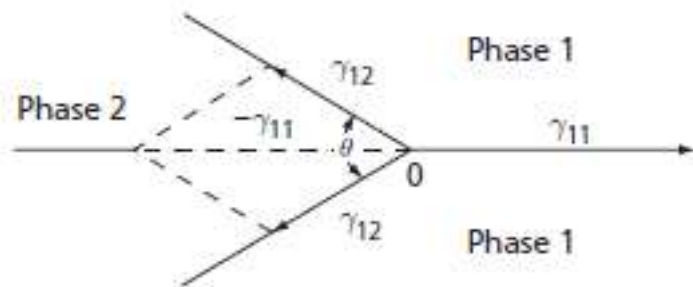
Contorno de grão com outras fases

FIG. 6.18 The grain-boundary surface tensions at a junction between two crystals of the same phase with a crystal of a different phase
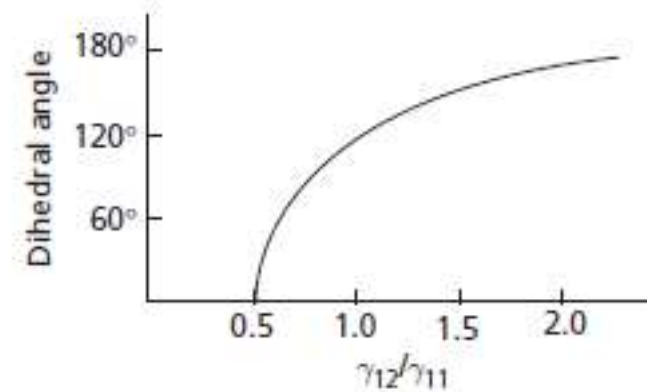

FIG. 6.19 The dependence of the two-phase dihedral angle on the ratio of the two-phase surface tension to the single-phase surface tension

$$\frac{\gamma_{12}}{\gamma_{11}} = \frac{1}{2 \cos \frac{\theta}{2}}$$
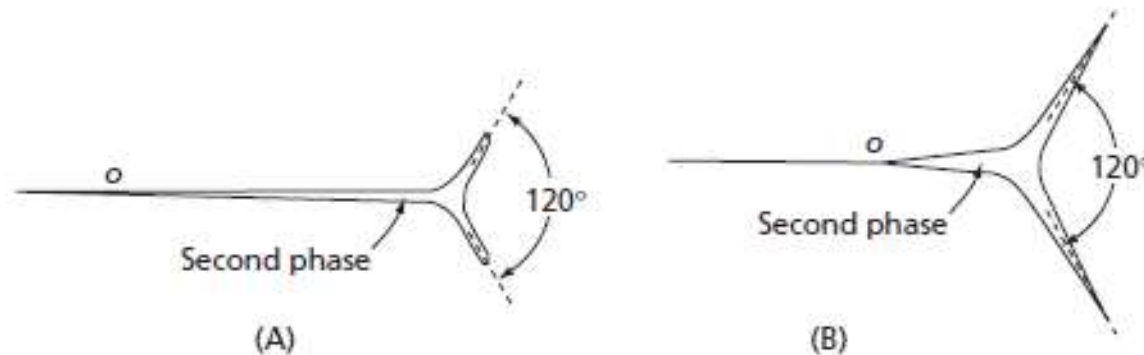
Contorno de grão com outras fases

FIG. 6.20 When the dihedral angle is small, the second phase (even if present in small quantities) tends to separate crystals of the first phase. (A) dihedral angle 1°, (B) dihedral angle 10°
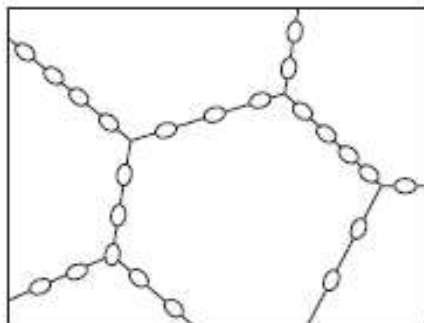

FIG. 6.21 When the dihedral angle is large (above 60°), the second phase (when present in small quantities) tends to form small discrete particles, usually in the boundaries of the first phase

$$\frac{\gamma_{12}}{\gamma_{11}} = \frac{1}{2 \cos \frac{\theta}{2}}$$
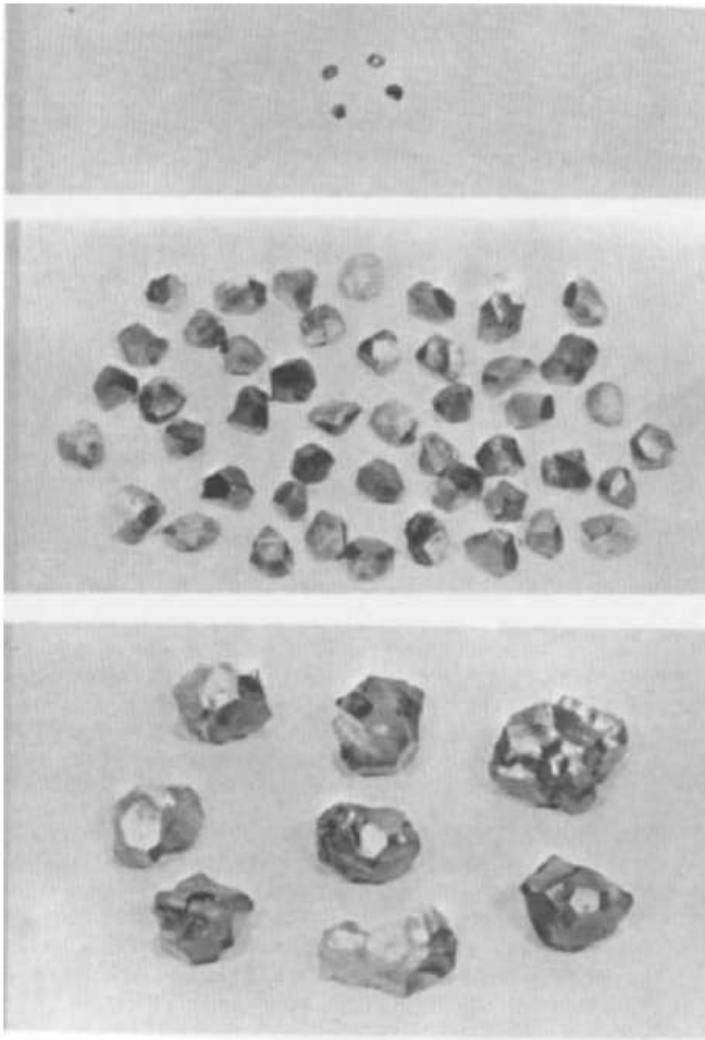
Tamanho de grão

FIG. 6.22 Grains removed from a beta brass specimen that appeared to be of a nearly uniform grain size on a metallographic section. Three of some 15 size classifications are shown in these photographs. They represent the smallest, the largest, and a size from the middle of the range. (The original photographs are from F. Hull, Westinghouse Electric Company Research Laboratories, Pittsburgh. Copies were furnished courtesy of K. R. Craig.)

$$\bar{l} = \frac{1}{\bar{N}_l}$$

$$S_v = 2\bar{N}_l$$

Equação de Hall-Petch
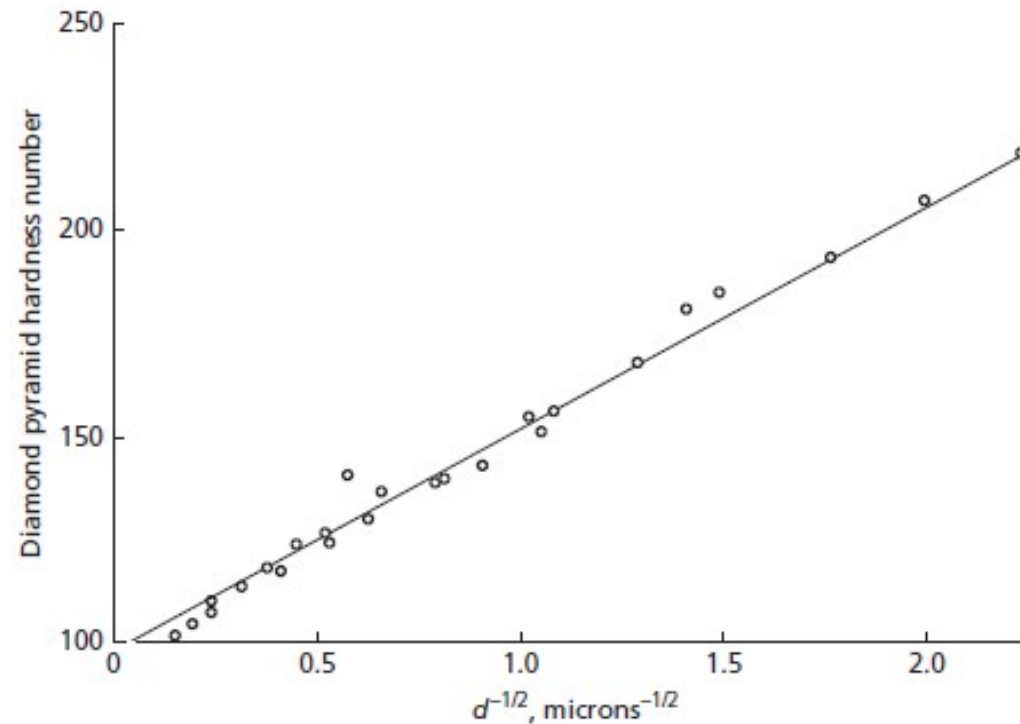
$$H = H_o + k_H d^{-1/2}$$

FIG. 6.23 The hardness of titanium as a function of the reciprocal of the square root of the grain size. (From the data of H. Hu and R. S. Cline, *TMS-AIME,* **242** 1013 [1968]. This data has been previously presented in this form by R. W. Armstrong and P. C. Jindal, *TMS-AIME,* **242** 2513 [1968].)

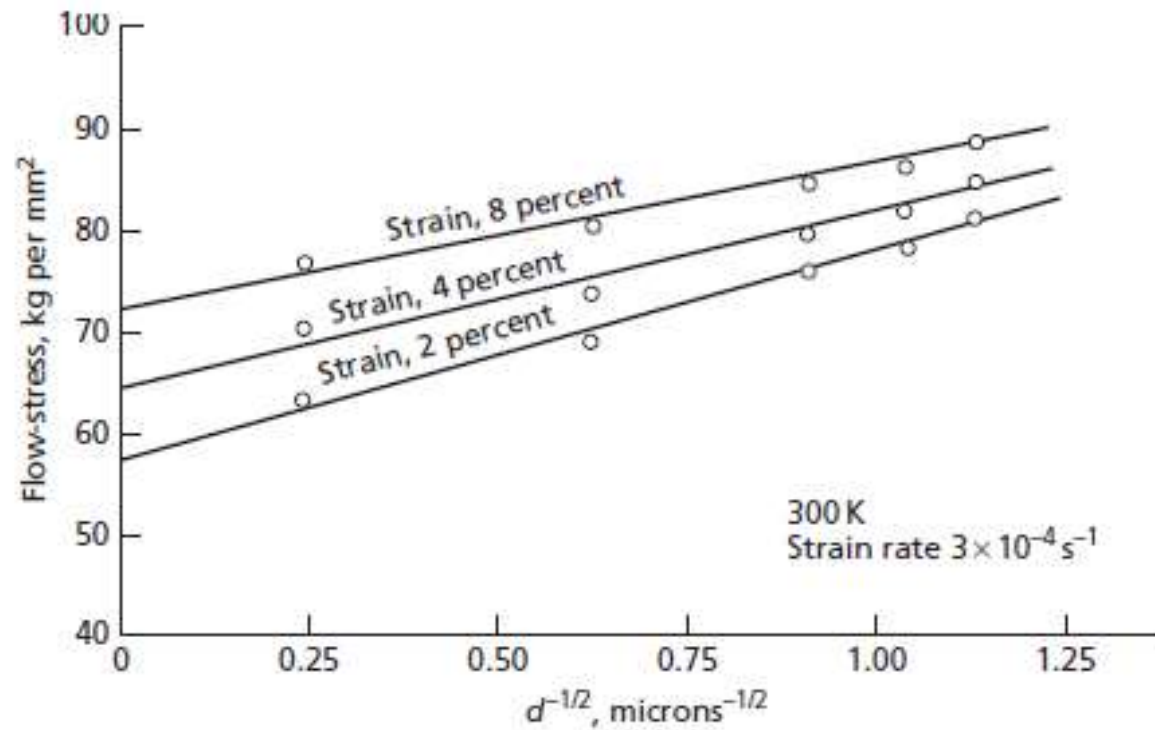# Equação de Hall-Petch

$$\sigma = \sigma_o + kd^{-1/2}$$

FIG. 6.24 The flow-stress of titanium as a function of the reciprocal of the square root of the grain size. (After Jones, R. L. and Conrad, H., TMS-AIME, 245 779 [1969].)
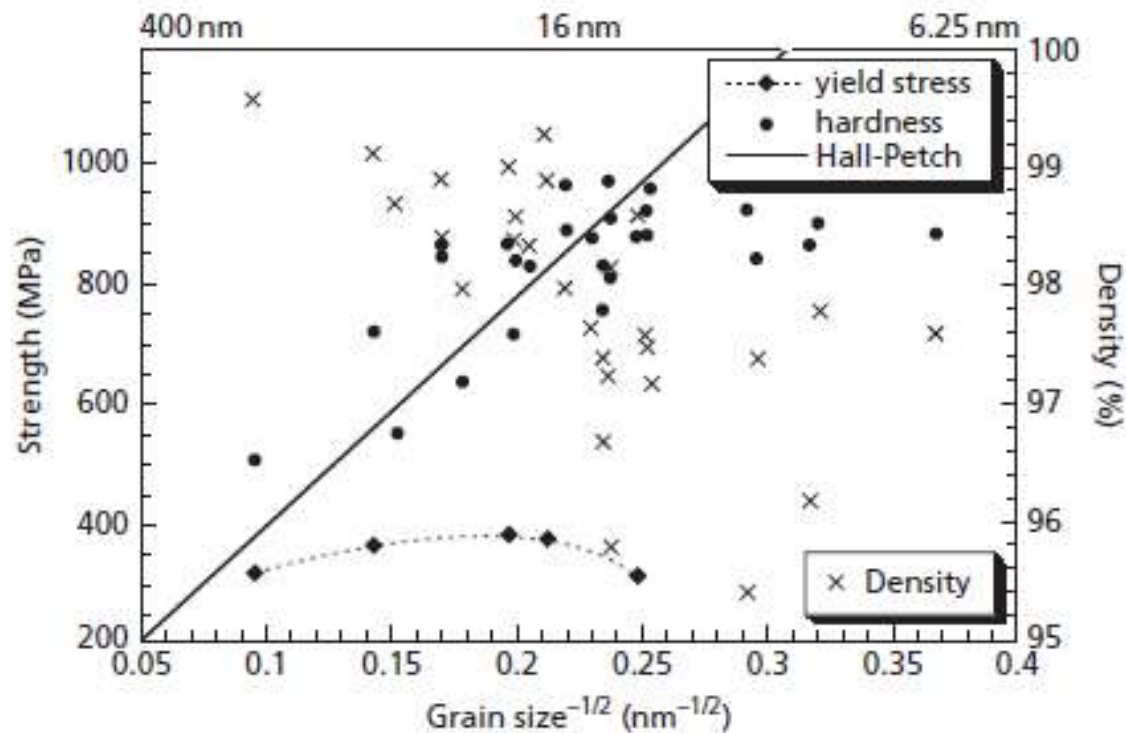
Metais nanocristalinos

FIG. 6.25 Plot of yield strength and Vickers microhardness (divided by 3) as a function of the inverse square root of the grain size. Also shown is an extrapolation to small grain sizes of the coarse-grained Hall-Petch relation for Cu and the change in the bulk density. (This material was published in Acta Materialia, Vol. 45, Issue 10, P. G. Sanders, J. A. Eastman and J. R. Weertman, Elastic and tensile behavior of nanocrystalline copper and palladium, 4019–4025. Copyright Elsevier Science Ltd. (1997). http://www.sciencedirect.com/science/journal/13596454)
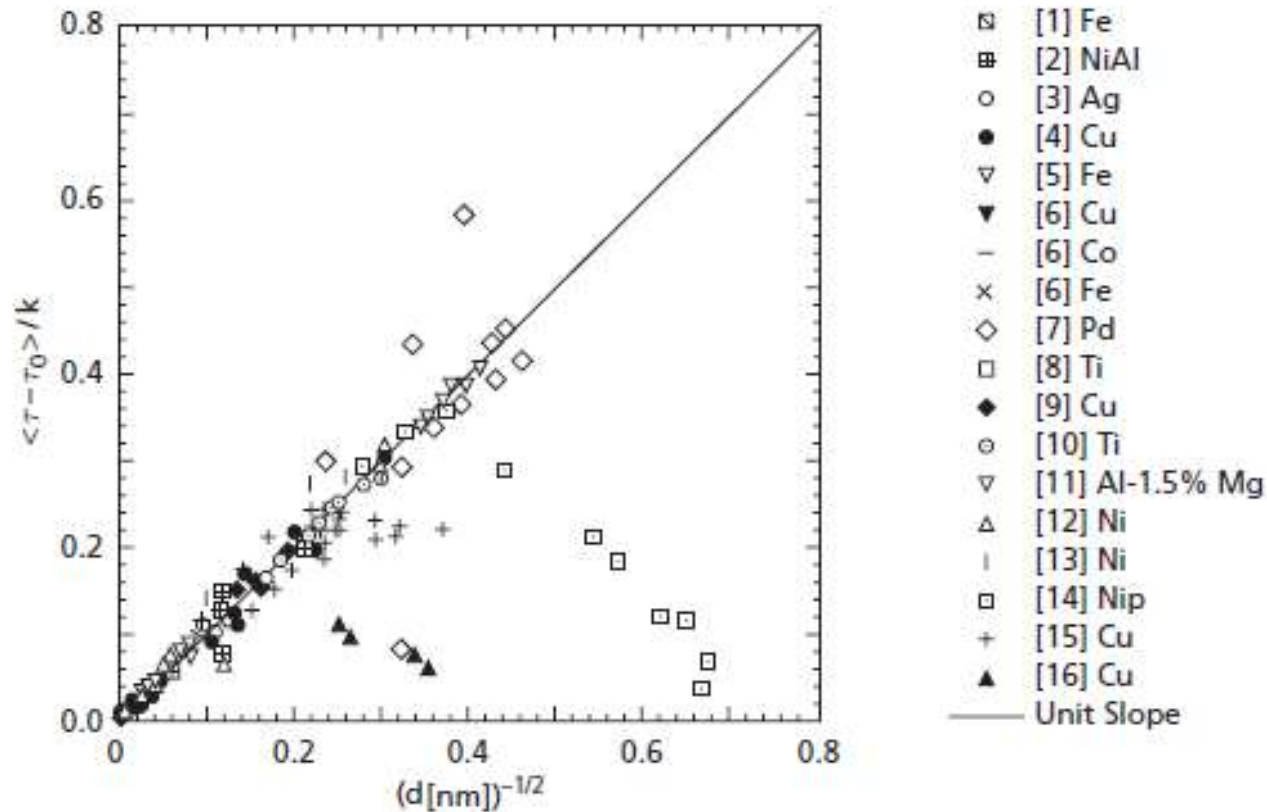
Metais nanocristalinos

FIG. 6.26 Compilation of yield stress data for several metallic systems. (This article was published in Acta Materialia, R. A. Masumura, P. M. Hazzledine and C. S. Pande, Vol. 46, No. 10, Yield Stress of Fine Grained Materials, pp. 4527–4534. Copyright Elsevier Science Ltd. (1998) http://www.sciencedirect.com/science/journal/13596454)

Contornos com coincidência de redes

O Net A
● Net B
◯ Coincidence sites
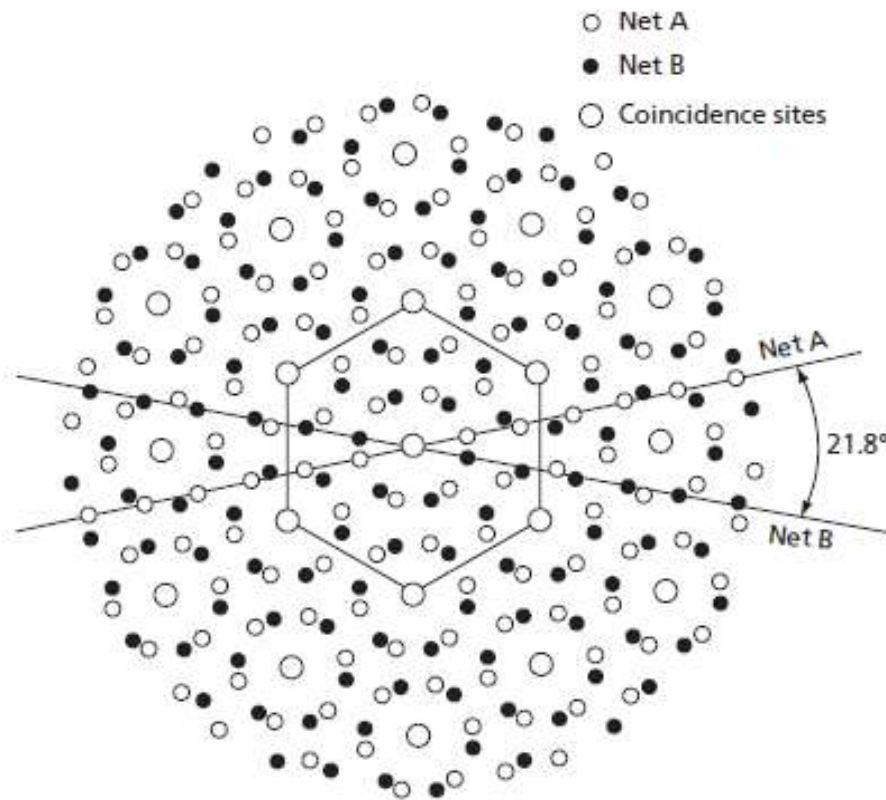
$$\theta = (2 \tan^{-1} (y/x))(N^{1/2})$$

$$\Sigma = x^2 + y^2 N$$

$$N = h^2 + k^2 + l^2$$

FIG. 6.27 A coincident site boundary obtained by a 22° rotation across a (111) plane (i.e., about a ⟨111⟩ axis). The reciprocal density, Σ, of the coincident sites, shown as large open circles, is 7. (After Kronberg and Wilson.)
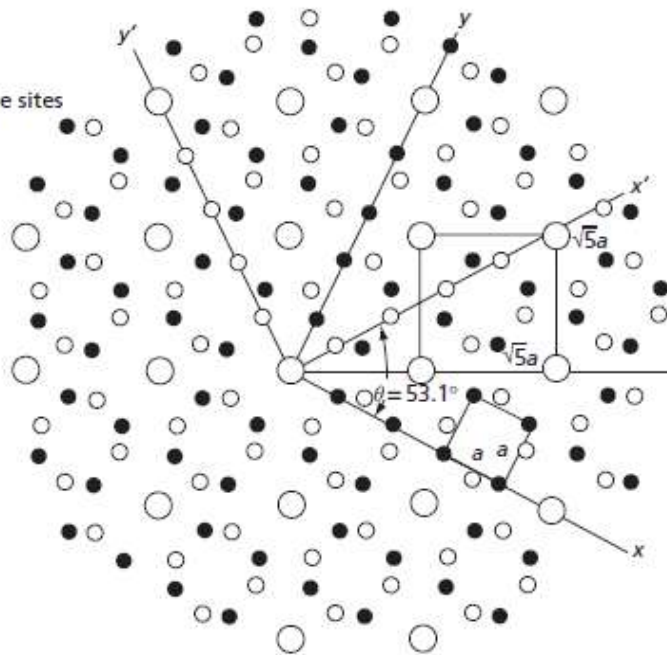
Contornos com coincidência de redes

FIG. 6.28 A rotation of 53.1° about a ⟨100⟩ axis of a simple cubic crystal gives this coincident site boundary with $\Sigma = 5$. The coincident sites also form a lattice with a unit cell whose sides are equal to $\sqrt{5}a$ in the boundary. The cell size of the reciprocal lattice is thus five times larger than that of the primitive lattice
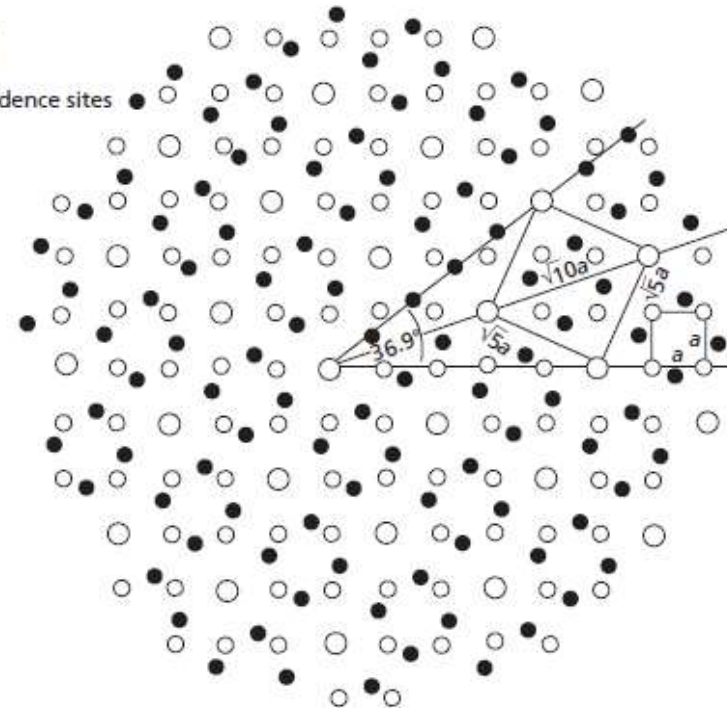
FIG. 6.29 A 36.9° rotation about a ⟨100⟩ axis also produces a coincident site boundary with $\Sigma = 5$ due to the symmetry of the simple cubic lattice
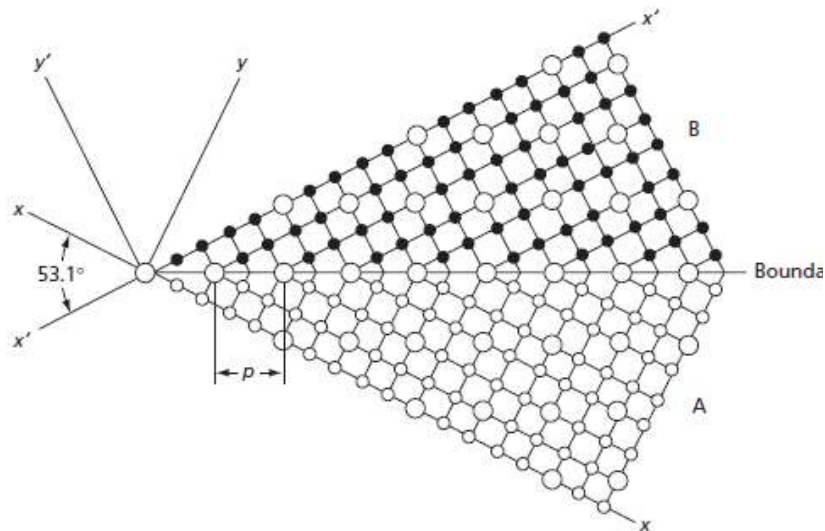
Contornos com coincidência de redes

FIG. 6.31 The coincident site boundaries in Figs. 6.27 to 6.29 are twist boundaries. This figure illustrates a coincident site boundary formed by a tilt of 53.1° about a ⟨100⟩ axis of a simple cubic crystal. Σ also equals 5 for this boundary and its structural periodicity, p, is equal to an edge of the coincident site lattice
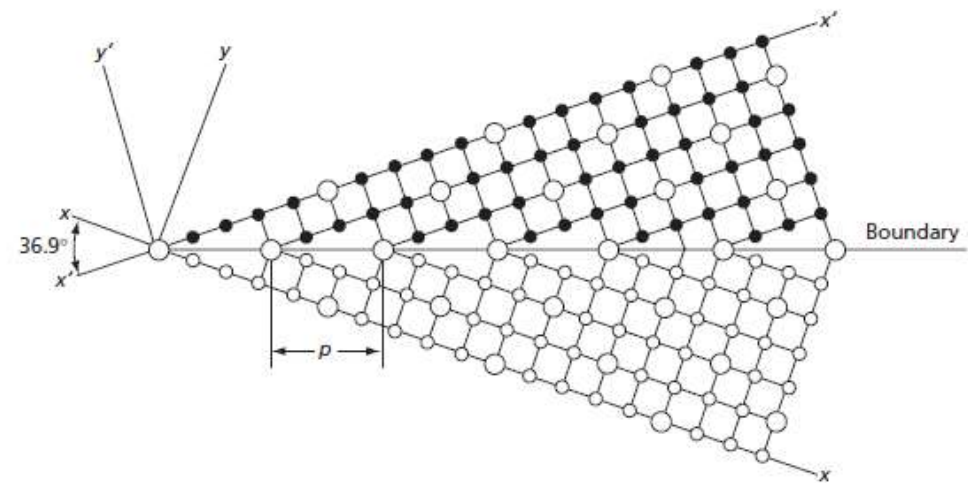
FIG. 6.32 A tilt of 36.9° about ⟨100⟩ of a simple cubic lattice also yields a coincident site boundary, but in this case the structural periodicity, p, is equal to the diagonal of the coincident site unit cell. Σ again is equal to 5
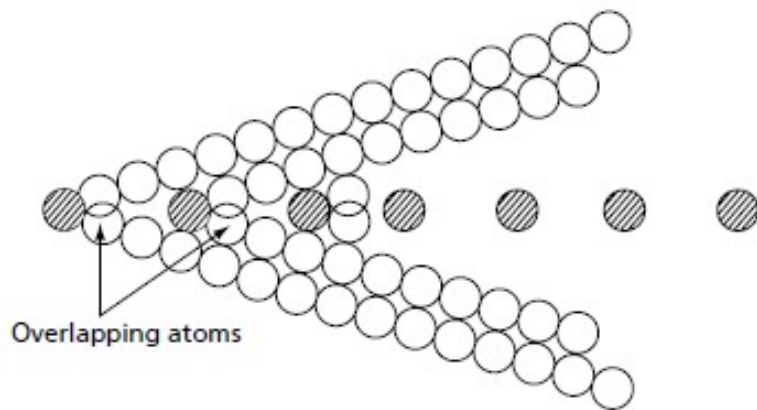
Contornos com coincidência de redes

FIG. 6.33 If the atoms of the diagram in Fig. 6.32 are drawn as hard balls instead of points, one finds that there is an overlap of the atoms just to the right of the coincident sites on the boundary
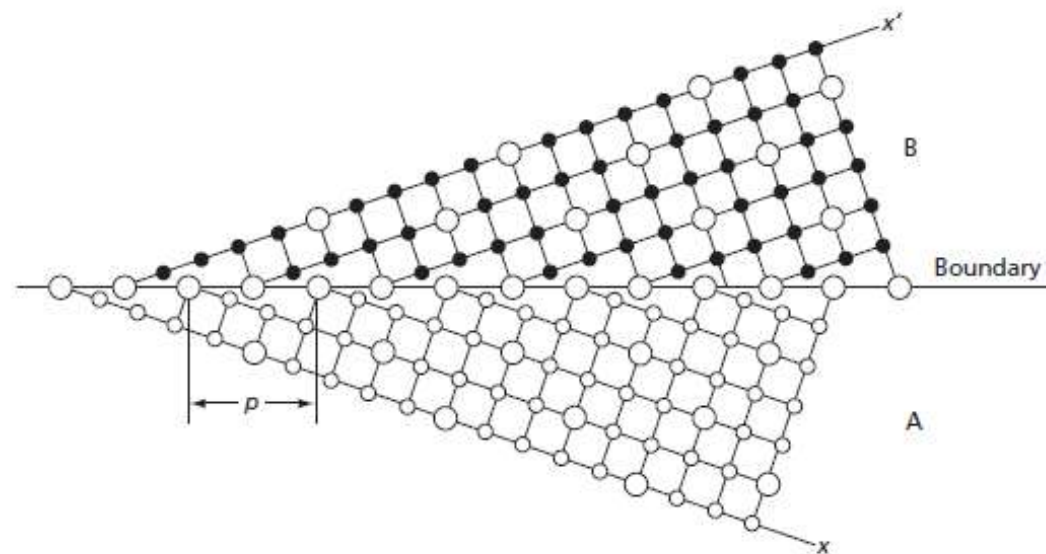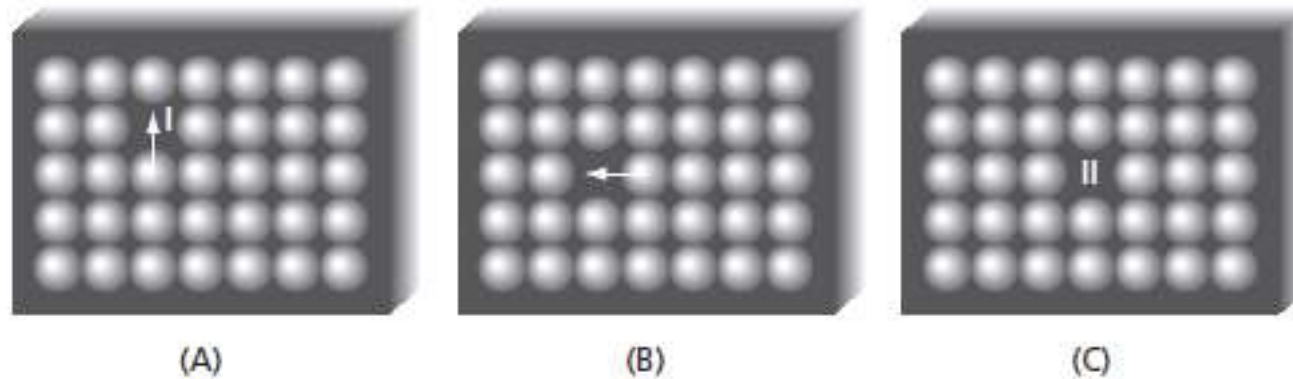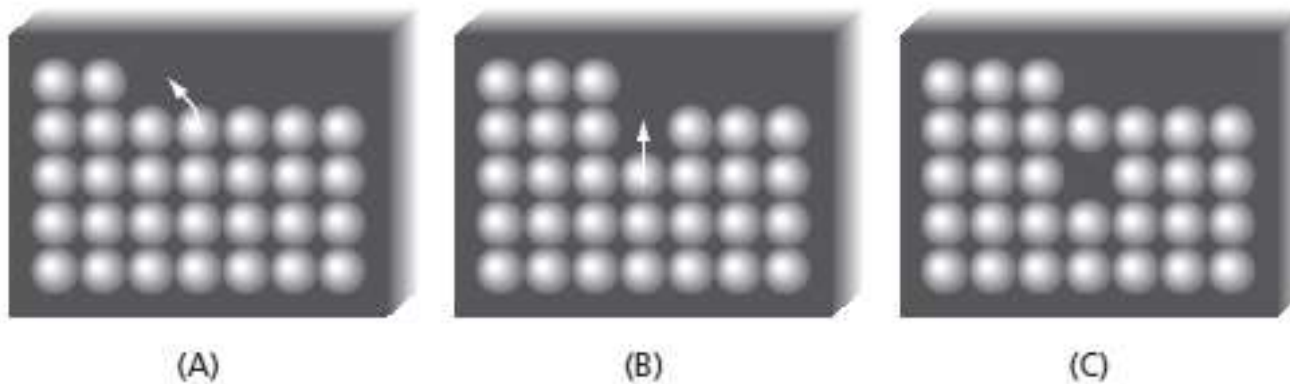
Overlapping atoms

FIG. 6.34 As suggested by Aust,[18] the overlapping of the atoms at the boundary could be relieved by a relative translation of the lattices above and below the boundary

Vacâncias

(A) (B) (C)

FIG. 7.1 Three steps in the motion of a vacancy through a crystal

$$\frac{n_v}{n_o} = e^{-w/kT}$$

(A) (B) (C)

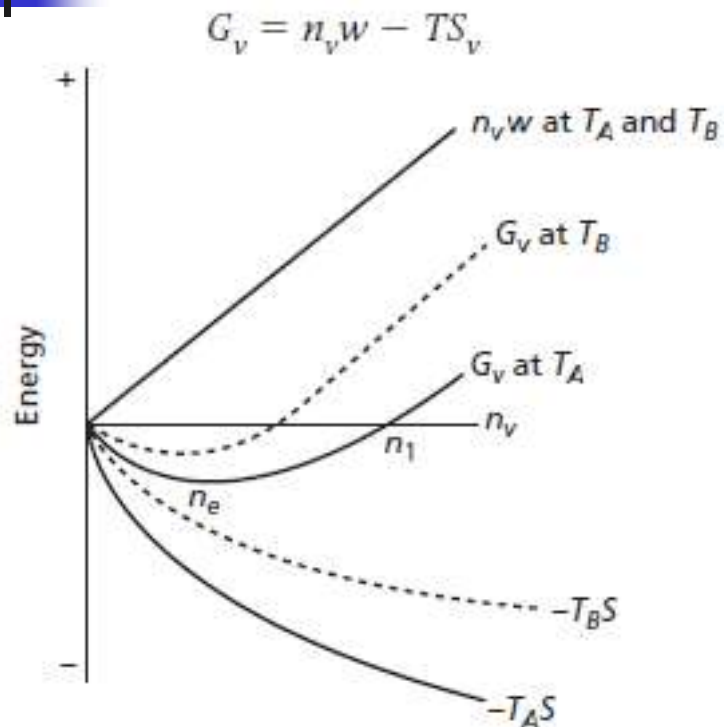**FIG. 7.2** The creation of a vacancy

$$\frac{n_v}{n_o} = e^{-H_f/RT}$$

Vacâncias

$$G_v = n_v w - TS_v$$

FIG. 7.4 Free energy as a function of the number of vacancies, n_v, in a crystal at a high temperature

$$X_c = \frac{n_v}{n_o} = e^{S_v/k} \cdot e^{-H_v/kT}$$

TABLE 7.1 Enthalpy and Entropy of Formation of Single Vacancy in Selected Metals.

Element	H_v (eV)	S_v (units of K)
Aluminum	0.60–0.77	0.7–1.76
Cadmium	0.39–0.47	1.5–2.8
Cobalt	1.34	—
Copper	1.04–1.31	1.5–2.8
Gold	0.89–1.0	1.1
Iron, bcc	1.4–1.6	—
Molybdenum	3.0–3.24	—
Niobium	$2.6 \geq 2.7$	—
Nickel	1.45–1.74	—
Platinum	1.15–1.6	1.3–4.5
Silver	1.09–1.19	—
Tungsten	3.1–4.0	2.3

Source: Wollenberger[5]
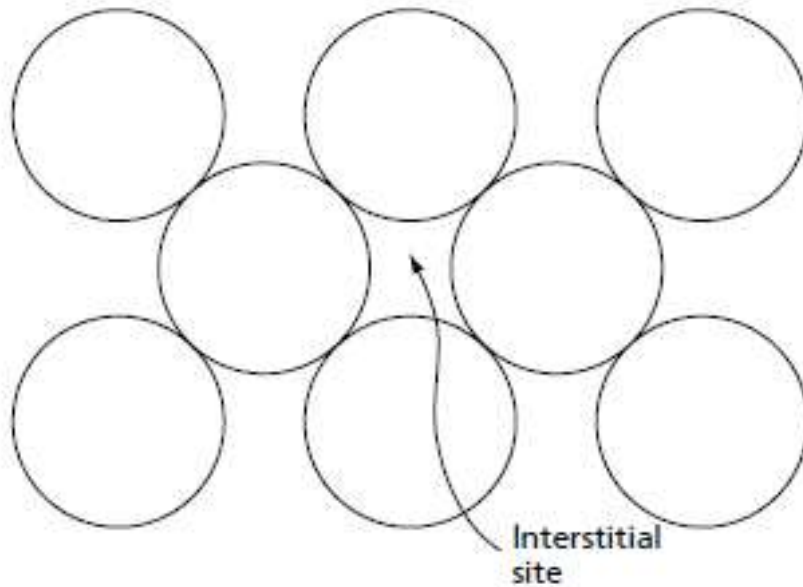
Movimentação de vacâncias
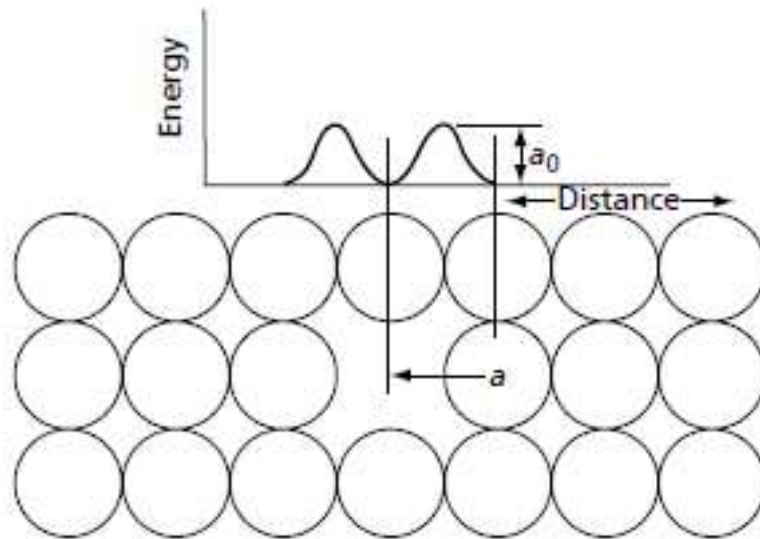
$$r_v = Ae^{-H_m/RT}$$

$$r_a = Ae^{-H_m/RT} \times e^{-H_f/RT} = Ae^{-(H_m+H_f)/RT}$$

FIG. 7.5 The energy barrier that an atom must overcome in order to jump into a vacancy

Vacância com Intersticial

Interstitial
site

4 eV p/ Cu

FIG. 7.7 The size of the interstitial site is much smaller than the size of the solvent atoms
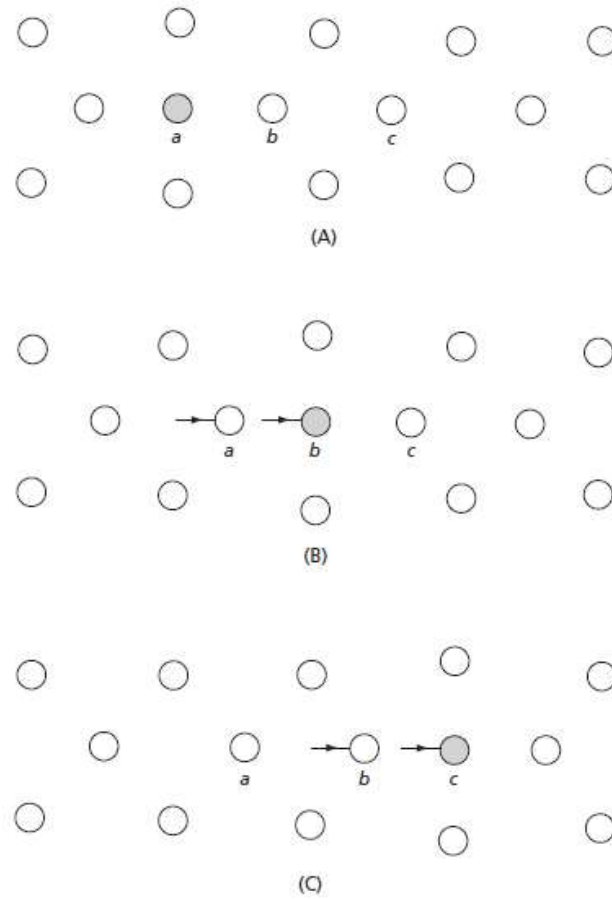
Mobilidade

FIG. 7.8 The configuration when an interstitial atom can move readily through the crystal

Divacâncias

$$\frac{n_{dv}}{n_v} = 1.2ze^{-q_b/kT}$$

0.3–0.4 eV in the case of copper.